Miner Petrol (2009) 96:43–58
DOI 10.1007/s00710-009-0047-4

ORIGINAL PAPER

Crystallisation conditions (T, P, fO_2) from mineral chemistry of Cu- and Au-mineralised alkaline intrusions in the Red River–Jinshajiang alkaline igneous belt, western Yunnan Province, China

Bi Xianwu · Hu Ruizhong · J. J. Hanley · J. E. Mungall · Peng Jiantang · Shang Linbo · Wu Kaixing · Suang Yan · Li Hongli · Hu Xiaoyan

Received: 15 February 2007 / Accepted: 6 February 2009 / Published online: 3 March 2009

Abstract The Oligocene Yao'an syenite porphyry, associated with gold mineralisation, and the Machangqing alkali granite porphyry–monzonite porphyry, associated with Cu mineralisation, belong to the Red River–Jinshajiang alkaline igneous belt that formed in a continental setting in southwestern China. A study of the mineral chemistry of major silicate minerals in these two mineralised intrusions provides insights into their overall crystallisation conditions. The temperature and pressure conditions, derived from amphibole–plagioclase and perthite–plagioclase geothermometry and Al-in-amphibole barometry, suggest that the Yao'an intrusion crystallised at around 820±50°C and 0.9–1.3 kbar, whereas the Machangqing intrusion crystallised at around 730±50°C and 2.2–2.8 kbar. The higher temperature and lower pressure of crystallisation for the Yao'an intrusion relative to the Machangqing intrusion indicates that it was emplaced at a shallower crustal level. Based on biotite composition, the two intrusions formed under imposed oxygen fugacities above the Ni–NiO buffer (NNO), and the Yao'an intrusion crystallised under more oxidising conditions than the Machangqing intrusion. The results show that the intrusions associated with Cu–Au mineralisation in the Red River–Jinshajiang alkaline igneous belt were emplaced at a relatively high fO_2, which, together with the weakly fractionated magma, favoured Au enrichment relative to Cu in the belt.

Editorial handling: L. Gwalani

B. Xianwu · H. Ruizhong · P. Jiantang · S. Linbo · W. Kaixing · S. Yan · L. Hongli · H. Xiaoyan
State Key Laboratory of Ore Geochemistry,
Institute of Geochemistry, Chinese Academy of Sciences,
73 Guanshui Road,
Guiyang 550002, China

J. J. Hanley · J. E. Mungall
Department of Geology, University of Toronto,
22 Russell Street,
Toronto, Canada M5S 3B1

W. Kaixing · S. Yan · L. Hongli · H. Xiaoyan
Graduate School of the Chinese Academy of Sciences,
Beijing 100039, China

B. Xianwu (✉)
46 Guanshui Road,
Guiyang City 550002, China
e-mail: bixianwu@vip.gyig.ac.cn

Introduction

Magmatic–hydrothermal Cu–Au deposits reveal a persistent genetic association with oxidised intrusions (Imai et al. 1993; Richards 1995; Sillitoe 1997, 2002; Ballard et al. 2002; Maughan et al. 2002; Pollard and Taylor 2002; Holliday et al. 2002). This association is built on the fact that convergent margin magmas associated with Cu–Au mineralisation have a relatively high fO_2 (Sun et al. 2004), which is due to high fO_2 melts and fluids released from subducted slabs, or to brine exsolution during magmatic evolution (Maughan et al. 2002). Therefore, oxidation state is a key factor in determining the potential of the convergent margin magmas to form Cu–Au mineralisation (Ballard et al. 2002; Mungall 2002; Richards 2003; Sun et al. 2004; Liang et al. 2006; Bonin 2007). In recent years, many magmatic–hydrothermal Cu–Au deposits, for example, epithermal/porphyry types, have been shown to be associated with

high-K calc-alkaline and alkaline magmas in continental tectonic settings: for example, the porphyry-type Cu–Au deposits in the Red River–Jinshajiang alkaline igneous belt, southwestern China, and the Dexing porphyry-type Cu deposits in eastern China (Hu et al. 1998, 2004; Bi et al. 2000, 2005; Hou et al. 2003, 2007; Rui et al. 2004). However, there have been few definitive studies (Liang et al. 2006) of the oxidation state of high-K calc-alkaline and alkaline magmas associated with Cu–Au mineralisation in continental tectonic settings. Therefore, it is of considerable scientific interest, to determine the magmatic oxidation state of such intrusions in continental tectonic settings.

Copper and Au-mineralised alkaline intrusions occur widely in the Red River–Jinshajiang alkaline igneous belt of Southwestern China. Examples include the Yulong and Machangqing intrusions associated with copper deposits (Hu et al. 1998, 2004; Hou et al. 2003), and the Yao'an, Beiya and Bengge intrusions associated with gold deposits (Bi et al. 2002, 2004). These mineralised intrusions are felsic, with SiO_2 ranging from 58.5 to 70.8 wt.%, K_2O+ Na_2O from 7.7 to 11.5 wt.% and $K_2O/Na_2O>1$, and ages of ~40–30 Ma (Zhang et al. 1997; Chung et al. 1998). The gold and copper deposits are located at both the exo- and endo-contact zones of the intrusions, and their ages also range from ~40 to 30 Ma (Wang et al. 2005). The ore-forming fluids of both gold and copper deposits were derived from the alkaline intrusions, but the magmatic fluids responsible for the gold deposits were less extensively diluted by modified air-saturated water (MASW) than those that deposited the copper deposits (Hu et al. 2004). Although some researchers have obtained geochemical and structural information for individual batholiths and suites of plutonic rocks within the Red River–Jinshajiang alkaline intrusive belt (Tu et al. 1984; Zhang et al. 1987, 1997; Leloup et al. 1995; Xie and Zhang 1995; Hu and Huang 1997; Deng et al. 1998; Wang et al. 1998; Bi, 1999; Zhang and Schärer 1999; Wang et al. 2001), constraints on magmatic evolution and mineralisation are not well understood. Thermobarometric data are particularly lacking from plutons of the Red River–Jinshajiang igneous belt. Liang et al. (2006) used the Ce(IV)/Ce(III) ratio in zircon to examine the oxidation state of the Yulong ore-bearing porphyries in the Red River–Jinshajiang alkaline igneous belt, and suggested that the ore-bearing porphyries crystallised from a relatively oxidised magma.

Estimation of the thermochemical characteristics during magma crystallisation can provide useful information on the nature of magmatic evolutionary processes. Chemical analysis of igneous rock-forming minerals has been widely used to estimate emplacement pressure, temperature, oxygen fugacity and compositional variations of igneous rocks. For example, the analysis and interpretation of plutonic rocks may be assisted by the application of feldspar thermometry (e.g., Fuhrman and Lindsley 1988), amphibole–plagioclase thermometry (e.g., Holland and Blundy 1994), biotite–apatite thermometry (e.g., Ludington 1978; Zhu and Serjensky 1991) and Al-in-amphibole barometry (e.g., Vyhnal et al. 1991; Ghent et al. 1991; Schmidt 1992; Anderson and Smith 1995; Ague 1997). Biotite and amphibole are very common constituents of igneous rocks, and contain both Fe^{+2} and Fe^{+3} whose ratio can be used to constrain T, P and fO_2 during magmatic evolution (Wones and Eugster 1965; Rowins et al. 1991; Loferski and Ayuso 1995; Stewart et al. 1996; Elliott et al. 1998; Stone 2000; Elliott 2001). Selby and Nesbitt (2000) examined the major-element chemistry of igneous biotite with the objective of distinguishing between mineralised and barren plutons. It has been suggested that the intrusive suites related to major Au–Cu porphyry and gold epithermal systems are especially oxidised relative to those suites related to copper porphyry or W–Mo porphyry systems (e.g., Ishihara 1981; Lowenstern 1991; Rowins et al. 1991; Sillitoe 1997; Garrio et al. 2002; Mungall 2002).

In this paper, whole-rock and mineral chemistry are used to study the crystallisation conditions of the Yao'an syenite porphyry associated with gold mineralisation, and the Machangqing alkali–granite porphyry associated with copper mineralisation, both located within the Red River–Jinshajiang alkaline igneous belt in western Yunnan Province, China, to understand the oxidation state of such intrusions associated with copper and gold mineralization in continental tectonic settings.

Geological setting

The Red River–Jinshajiang alkaline igneous belt is adjacent to the Red River–Jinshajiang fault zone in the eastern part of the Tibetan plateau, the eastern part of which comprises several terranes: from north to south, the Songpan–Ganze, Qiangtang, Lhasa and Yangtze terranes (Fig. 1), which were welded together prior to the Cretaceous to form part of the Eurasian plate. At ~60–70 Ma, the India–Eurasian collision created the plateau and resulted in eastward extrusion tectonics faciltated by strike–slip motion along the NW–WNW trending Red River–Jinshajiang fault zone (Zhang et al. 1987; Turner et al. 1996; Chung et al. 1997, 1998; Bi 1999; Yin and Harrison 2000). Numerous alkaline igneous bodies occur along or near the fault zone (Fig. 1), forming a magmatic belt over 1000 km long and generally 50–80 km wide. K–Ar and Ar–Ar dating of whole-rock or mineral samples from the alkaline rocks define intrusion ages of ~40–30 Ma (Zhang et al. 1997; Chung et al. 1998; Liang et al. 2006). The alkaline rocks are exposed around two tectonic belts, the Red River shear zone (RRSZ) and the Jinshajiang fault system (Fig. 1a). Geochemically, these

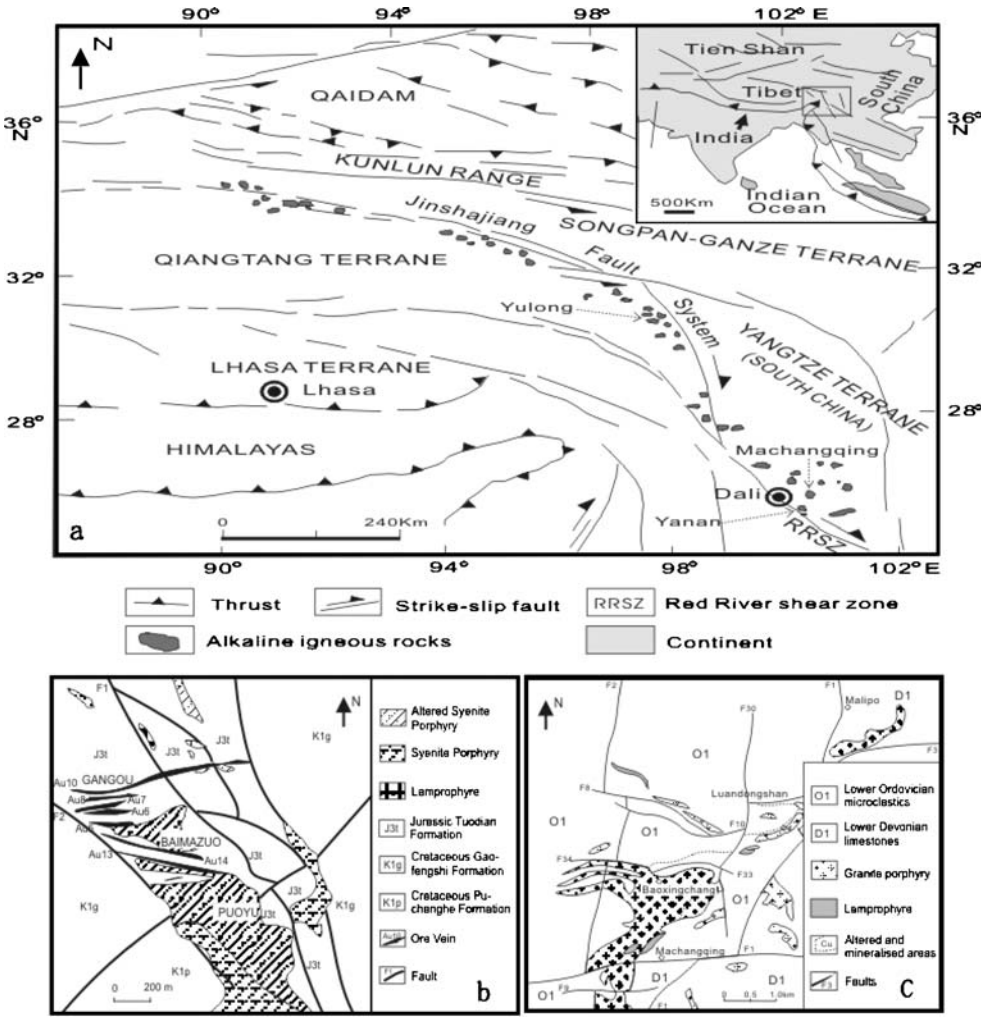

Fig. 1 **a** A sketch geological map of the Red River–Jinshajiang fault zone showing the locations of alkaline igneous rocks and related ore deposits (modified from Chung et al. 1998); **b** a sketch map of the Yao'an alkaline intrusion (modified from Bi et al. 2005); **c** a sketch map of the Machangqing alkaline intrusion (modified from Bi 1999)

volcanic and intrusive rocks range from basaltic to trachytic and rhyolitic in composition (Chung et al. 1998). They show ultra-potassic or shoshonitic character and incompatible trace-element patterns with highly enriched large-ion lithophile elements and light rare-earth elements, and marked depletions in the high field strength elements, such as Nb, Ta and Ti (Chung et al. 1998; Hou et al. 2003; Bi et al. 2005). The Sm–Nd isotopic compositions of these volcanic and intrusive rocks (Zhang et al. 1997; Bi et al. 2005) indicate that they were derived from an enriched mantle source (EMII). The above features support the origin of these alkaline magmas in a metasomatised lithospheric mantle which was previously contaminated by fluids or melts derived from a subducted oceanic slab (Chung et al. 1998; Hou et al. 2003). A series of Tertiary rifted basins, the eruption of alkaline basalt, and the positive gravity anomaly pattern along the Red River–Jinshajiang fault system, suggest that the alkaline rocks formed in a post-collisional extensional setting (Zhang et al. 1987; Turner et al. 1996; Chung et al. 1997, 1998; Hou et al. 2003).

Geology and geochemistry of the intrusions

The Yao'an alkaline stock in Yao'an County, Nanhua County and Mouding County, Yunnan Province, was emplaced primarily into dark-gray silty mudstones and marl of Jurassic age (Fig. 1b). The intrusion appears as stocks and apophyses of syenite porphyry, subordinate quartz syenite porphyry and minor occurrences of lamprophyre. The Machangqing alkaline intrusion within the bounds of Xiangyun County, Yunnan Province, predominantly intruded into lower Ordovician microclastic rocks and Devonian limestones (Fig. 1c). The intrusion appears as stocks of alkali–granite porphyry and monzonite porphyry. Table 1 summarises the characteristics of the Yao'an syenite porphyry and Machangqing alkali–granite porphyry. The data presented in Table 1 illustrate some differences between the two intrusions with respect to textural, mineralogical and chemical composition, although they have a similar tectonic setting, age of emplacement, and magma source region.

The Yao'an hydrothermal gold mineralisation occurs within and around the Yao'an syenite porphyry. The syenite

Table 1 Characteristics of the Yao'an and Machangqing alkaline intrusions (data from Bi 1999; Bi et al. 2005; Zhang et al. 1997; Peng et al. 2005)

	Yao'an alkaline intrusion	Machangqing alkaline intrusion
Host rocks	Dark-gray silty mudstones and marl of Jurassic Tuodian Formation	Lower Ordovician microclastics and Lower Devonian limestones
Outcrop area	<1 km^2	1.3 km^2
Occurrence	Stocks and apophyses	Stocks
Intrusion type	Syenite porphyry	Granite porphyry
	Quartz syenite porphyry	Monzonite porphyry
	Lamporphyre	
Mineral phenocryst	Kfs+Pl+Cpy+Amph+Bi	Kfs+Pl+Amph+Bi+Qtz
	Typically euhedral	Euhedral to subhedral
	Size=1–10 mm	Size=0.5–10 mm
	35–50 vol.% of whole rock	30–45 vol.% of whole rock
Mafic mineral	Cpx+Amph+Bi	Amph+Bi
Accessory mineral assemblage	Ap+Ms+Tit+Zr	Ap+Ms+Tit+Zr
Chemical composition	SiO_2=58.5–67.1%	SiO_2=66.9–70.8%
	CaO=2.30–5.80%	CaO=1.20–3.30%
	K_2O+Na_2O=8.1–10.0%	K_2O+Na_2O=7.7–9.4%
	K_2O/Na_2O=1.01–4.53	K_2O/Na_2O=1.02–2.05
	A/CNK=0.79–1.09	A/CNK=0.87–1.16
	FeO total=3.5 wt.%	FeO total=2.4 wt.%
	MgO/(FeO total+MgO)=0.26–0.43	MgO/(FeO total+MgO)=0.19–0.43
	∑REE=546.1–811.2 ppm	∑REE=213.6–257.9 ppm
	$(La/Yb)_N$=66.7–97.9	$(La/Yb)_N$=26.6–33.8
	I_{Sr}=0.7088–0.7093	I_{Sr}=0.7061–0.7082
	ε_{Nd}=−9.2 to −10.6	ε_{Nd}=−3.1 to −10.2
Age (average value)	33.5±1.0 Ma (Ar–Ar, Amph, Zhang et al. 1997)	33.7±1.0 Ma (Ar–Ar, Q, Peng et al. 2005)
Tectonic setting	The Red-River shear zone	The Red-River shear zone
Mineralization	Au–Ag–Pb–Cu	Cu–Mo–Au
Mineralization scale	10 t Au	20 t Cu
Ore grade	4–5 g/t Au	0.5 wt.% Cu
Origin	Hydrothermal deposit	Hydrothermal deposit

Amph tremolite, *Ap* apatite, *Bi* biotite, *Kfs* K-feldspar, *Ms* magnetite, *Pl* plagioclase, *Cpx* diopside, *Qtz* quartz, *Tit* titanite, *Zr* zircon, *A/CNK* molecular $Al_2O_3/(CaO+Na_2O+K_2O)$

porphyries in the mineralised area exhibit various degrees of hydrothermal alteration. Away from the orebody, the syenite porphyry is only very weakly altered with primary perthite, plagioclase, biotite and hornblende. Minor calcite is the product of hydrothermal alteration, and the proportion of altered minerals is less than 10 vol.%. Close to the orebody, however, the syenite porphyry is heavily altered: primary perthite is partially replaced by secondary K-feldspar. The alteration assemblages have been classified as K-feldspar alteration, sericitisation and propylitisation. In the proximal part the proportion of altered minerals is generally more than 50 vol.%. The Yao'an hydrothermal gold deposit is estimated to contain about 10 t of Au, with the average ore grade being 4–5 g/t (No. 304 Team of Southwest Geological Exploration Bureau 1995). The orebodies occur in the endo- and exo-contact zones of the Yao'an intrusion and the Jurassic Tuodian Formation. The orebodies mostly comprise veins, and are lenticular in shape, with branching and pinching common. The Yao'an gold deposit formed during two stages: an early sulfide (pyrite–chalcopyrite–galena) stage, and a later sulfide-oxide stage (pyrite–specularite). The stable isotope (S, C) and REE data suggest that the early sulfide stage mineralization of the Yao'an gold deposit was caused by orthomagmatic fluids derived from the Yao'an alkaline intrusions (Bi et al. 2004).

The Machangqing copper mineralisation occurs within and around the Machangqing intrusion. About 200,000 t of

Cu was estimated, with the average ore grade being 0.5% (No. 301 Team of Southwest Geological Exploration Bureau 1981). The orebodies are controlled structurally and occur as veins and fine disseminations in granite porphyries, contact hornfels in the Lower Ordovician metasedimentary rocks, and as skarns in the Devonian limestones. Porphyry-type and skarn-type ores constitute two major mineralisation styles in the Machangqing copper deposit. The Machangqing intrusive body exhibits strong hydrothermal alteration that forms more or less concentric zones extending outward from the inner part of the intrusion, including a silicification zone, K-silicate zone, propylitic zone and argillic zone. The silicification zone is characterised by veins and stockworks of quartz. The K-silicate zone is characterised by pervasive alteration of plagioclase to orthoclase, hornblende and primary biotite to secondary biotite. The alteration was accompanied by disseminated and veinlet-type Cu-sulfide mineralization. Propylitic alteration is weak but pervasive forming a wide halo in the country rocks and overprinting the other alteration zones. The main assemblage consists of epidote, chlorite, albite and calcite. Weak argillic alteration is characterised by the replacement of biotite and feldspar by clay minerals. The He, Ar, S and C isotopic data suggest copper mineralisation was apparently caused by orthomagmatic fluids derived from the Machangqing alkaline intrusion (Hu et al. 1998; Bi 1999; Bi et al. 2000).

Compositional evolution and fractional crystallisation of the magmas

The compositional evolution of the granitoids can be deduced from trace element abundances of mantle incompatible elements, and ratios between incompatible and compatible elements. Each parameter in turn is dependant, however, on processes, such as melting, mixing, crystallisation and fractionation, in addition to source characteristics. The K/Rb ratio is more useful in this regard as a measure of relative compositional evolution. Both K and Rb substitute into the same site in a range of minerals, but Rb to a lesser extent than K on account of its larger ionic radius, so Rb is progressively enriched in residual melts. Granitoids with K/Rb ratios under 140 are considered highly fractionated (Blevin 2004). K/Rb ratios are also useful in highly fractionated melts near minimum melting conditions, which may show a steep decrease in K/Rb ratio (Blevin 2004). As shown in Fig. 2, the Yao'an syenites, with K/Rb ratios greater than 150, can be regarded as being compositionally less evolved, whereas the Machangqing alkaline granites, with K/Rb ratios between 150 and 50, are more fractionated.

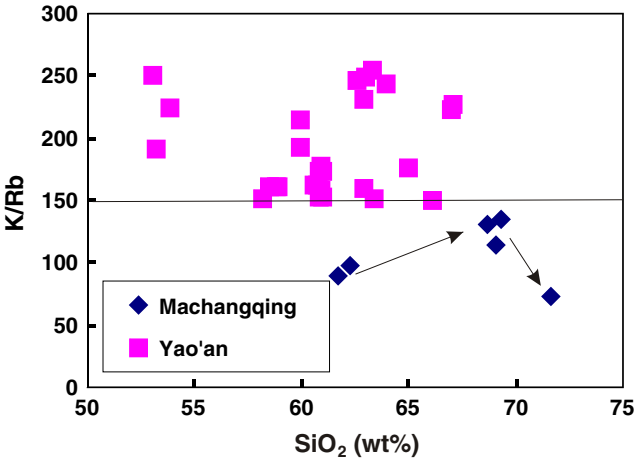

Fig. 2 K/Rb vs. SiO_2 plot for Yao'an and Machangqing alkaline intrusions

Mineral chemistry

Analytical methods

Minerals were analysed using wavelength dispersive X-ray spectrometry at the Department of Geology, University of Toronto, Canada. Mineral analyses were done using a CAMECA SX50 electron microprobe using 20 KV accelerating voltage, a static (fixed) beam (5 μm spot size), and a beam current of 25 nA for all elements other than F and Cl, which were analysed at a 60 nA beam current. On-peak counting times were 30 s for F and Cl and 10 s for all other elements. Calibration was performed using the following natural and synthetic standards: Si, Ca–wollastonite, Ti–rutile (synthetic), Al–corundum (synthetic), Mg–magnesium oxide (synthetic), Fe–hematite, Mn–rhodochrosite, Na–albite, K–sanidine, Cr–chromium III oxide (synthetic), Cl–tugtupite, and F–fluorite. Raw data were reduced using the software package Probe for Windows© (J. Donovan, Advanced Microbeam, Inc.) which uses standard ZAF correction algorithms during data reduction. Mineral formulae were recalculated using the software package MinPet© or using spreadsheet routines. Analytical accuracy was monitored by analysing glass of tugtupite composition, basaltic glass, and F-bearing phlogopite standards. Results are accurate to within 5% for all elements other than F which is within 20%. Routine detection limits (considered to be three standard deviations above background) were 0.05 and 0.008 elemental wt.% for F and Cl, respectively, and 0.02 elemental wt.% for all other elements. Presented here are 43 analyses of biotite, 15 analyses of tremolite and 18 analyses of feldspar from the Yao'an and Machangqing intrusions.

The calculation of Fe^{3+} in biotite from incomplete electron microprobe analyses is not a valid procedure

Table 2 Representative electron microprobe analyses of biotite from Yao'an syenite

	5-1core	5-1rim	3-1core	3-1rim	1-1core	1-2core	8-1core	9-1core	9-2core	9-3rim	3-1core	5-1	5-1′	5-1core	10-1	11-1	11-1core	11-2core
SiO_2	37.31	37.21	37.39	37.10	36.59	37.38	37.57	35.93	37.59	37.07	36.69	37.06	38.82	37.15	37.33	37.14	36.44	36.54
TiO_2	4.00	4.11	3.93	4.05	3.90	3.95	3.67	4.08	4.06	3.98	4.02	4.08	3.84	3.88	3.93	3.79	4.14	4.06
Al_2O_3	13.42	13.22	13.10	13.01	13.18	13.34	12.90	13.70	13.23	13.38	13.08	13.54	13.68	13.56	13.22	12.89	12.84	12.92
Cr_2O_3	<0.02	<0.02	0.03	<0.02	0.05	0.01	0.01	0.00	0.06	<0.02	<0.02	0.13	0.01	<0.02	<0.02	0.04	<0.02	0.01
FeO^T	14.56	12.54	15.41	13.57	16.23	13.11	15.73	15.63	14.07	13.56	14.79	12.99	11.59	15.66	15.17	15.43	15.30	16.11
MnO	0.27	0.23	0.20	0.22	0.21	0.23	0.16	0.09	0.20	0.14	0.22	0.18	0.14	0.24	0.25	0.21	0.17	0.21
MgO	15.72	17.22	16.04	16.83	14.85	17.11	15.25	14.51	16.55	16.80	15.87	17.36	17.66	15.79	15.82	15.53	15.57	14.65
CaO	0.04	0.01	0.01	0.00	0.01	0.00	0.00	0.00	0.00	0.01	0.02	0.10	0.07	0.03	0.05	0.06	0.03	0.05
Na_2O	0.62	0.59	0.59	0.76	0.54	0.60	0.56	0.57	0.61	0.56	0.66	0.65	0.83	0.52	0.63	0.61	0.59	0.59
K_2O	9.16	9.20	9.29	9.11	8.96	9.18	9.17	8.86	9.35	9.35	9.17	9.20	9.20	9.31	9.37	9.28	9.09	9.17
F	3.60	3.74	3.26	3.21	2.16	3.69	2.35	3.22	4.11	4.03	3.54	3.99	4.03	3.26	3.27	1.76	3.24	2.28
Cl	0.22	0.18	0.20	0.20	0.21	0.15	0.23	0.16	0.18	0.21	0.20	0.23	0.22	0.19	0.21	0.17	0.21	0.21
Total	98.90	98.26	99.45	98.07	96.87	98.74	97.59	96.75	100.01	99.09	98.26	99.49	100.09	99.56	99.26	96.91	97.61	96.80
FeO (wt.%)[a]							8.75	8.69	7.83	7.54	8.23	7.22	6.45	8.71	8.43	8.58	8.51	8.96
Fe_2O_3 (wt.%)[a]							6.98	6.94	6.25	6.02	6.57	5.77	5.15	6.95	6.73	6.85	6.79	7.15
$Fe^{3+}/(Fe^{3+}+Fe^{2+})$[a]							0.425	0.425	0.425	0.425	0.425	0.425	0.425	0.425	0.425	0.425	0.425	0.425
Fe^{3+}/Fe^{2+a}							0.739	0.739	0.739	0.739	0.739	0.739	0.739	0.739	0.739	0.739	0.739	0.739
Fe-ratio[a]	0.34	0.29	0.35	0.31	0.38	0.3	0.37	0.38	0.32	0.31	0.34	0.3	0.27	0.36	0.35	0.36	0.36	0.38
Mg-ratio[a]	0.66	0.71	0.65	0.69	0.62	0.7	0.63	0.62	0.68	0.69	0.66	0.7	0.73	0.64	0.65	0.64	0.64	0.62

[a] Fe-ratio=Fe/(Fe+Mg); Mg-ratio=Mg/(Fe+Mg); $Fe^{3+}/(Fe^{3+}+Fe^{2+})$ was determined by Mossbauer studies; $Fe^{3+}/Fe^{2+}=0.425/(1-0.425)$; $FeO(wt.\%)=wt.\%FeO^T/(1.08\times(Fe^{3+}/Fe^{2+})+1)$; $Fe_2O_3(wt.\%)=wt.\%FeO^T-wt.\%FeO$

Table 3 Representative electron microprobe analyses of biotite from Machangqing alkali granite

	39-6 1core	39-6 2core	39-6 1rim	39-6 2rim	39-3 core	39-3 rim	39-2 core	39-4 core	39-4 1rim	39-4 2rim	39-6 3	39-6 4	39-6 5	39-6 6	39-5 1	38-1 core	38-1 rim	38-3 core	38-3 inter	38-3 rim	38-5 rim	38-1 2	38-1 3	38-1 4	38-1 5
SiO_2	36.60	36.29	36.90	36.68	34.53	34.62	34.44	34.25	34.74	34.56	34.62	34.86	34.56	34.44	34.48	35.93	35.98	35.93	36.28	36.41	36.29	37.01	37.72	37.11	36.50
TiO_2	3.55	3.41	3.37	3.49	2.89	3.29	3.18	3.31	3.14	3.25	3.51	3.35	3.14	3.32	3.51	3.41	3.43	3.63	3.51	3.65	3.07	3.15	2.02	3.16	2.65
Al_2O_3	13.40	13.42	13.39	13.28	14.34	14.20	14.20	14.17	14.11	14.12	14.27	13.92	13.73	14.21	14.52	13.38	13.40	13.28	13.30	13.14	13.01	13.04	12.44	12.99	13.47
Cr_2O_3	<0.02	0.07	0.03	<0.02	0.06	<0.02	0.13	0.02	0.04	<0.02	<0.02	0.01	0.01	0.01	0.01	0.02	<0.02	0.04	<0.02	0.06	0.03	<0.02	0.01	<0.02	0.03
FeO^T	16.05	16.26	16.34	16.26	17.42	17.54	16.68	16.60	16.31	16.51	17.64	16.85	15.79	17.10	17.53	15.63	15.79	15.95	16.29	15.07	15.46	15.33	14.05	16.36	15.28
MnO	0.08	0.07	0.03	0.10	0.05	0.14	0.06	0.18	0.10	0.09	0.11	0.13	0.25	0.19	0.16	0.26	0.22	0.24	0.26	0.19	0.32	0.18	0.24	0.58	0.22
MgO	15.08	14.91	15.30	14.89	14.17	14.15	14.33	13.95	14.30	14.06	13.45	13.75	14.51	14.22	13.30	15.18	15.24	15.14	15.14	15.38	15.70	15.72	16.61	15.11	15.99
CaO	0.03	0.01	0.01	0.01	0.00	0.04	0.02	0.04	0.03	0.06	0.00	0.29	0.55	0.13	0.07	0.00	0.04	0.00	0.02	0.01	0.07	0.05	0.04	0.00	0.06
Na_2O	0.11	0.10	0.14	0.12	0.09	0.08	0.09	0.04	0.13	0.08	0.11	0.09	0.06	0.07	0.09	0.08	0.14	0.12	0.11	0.08	0.08	0.08	0.06	0.05	0.05
K_2O	9.80	9.86	9.67	9.66	9.68	9.33	9.21	9.72	9.63	9.44	9.67	9.24	8.74	9.04	9.03	9.88	9.87	9.88	10.00	9.94	9.86	10.03	9.77	9.87	8.57
F	0.94	1.03	0.82	0.95	0.65	0.76	0.87	0.54	0.82	0.74	0.69	1.08	0.86	0.83	0.72	1.86	2.09	1.53	1.39	1.89	1.98	2.41	2.27	1.77	1.63
Cl	0.16	0.10	0.09	0.13	0.04	0.06	0.05	0.11	0.04	0.07	0.12	0.12	0.10	0.07	0.10	0.12	0.11	0.13	0.15	0.09	0.15	0.17	0.12	0.09	0.09
Total	95.80	95.51	96.08	95.57	93.93	94.20	93.27	92.91	93.38	92.98	94.17	93.71	92.29	93.63	93.51	95.73	96.31	95.88	96.44	95.91	96.01	97.16	95.35	97.08	94.53
FeO (wt.%)[a]	9.77	9.90	9.95	9.90	10.61	10.68	10.15	10.10	9.93	10.05	10.74	10.26	9.62	10.41	10.67										
Fe_2O_3 (wt.%)[a]	6.28	6.36	6.39	6.36	6.81	6.86	6.52	6.49	6.38	6.46	6.90	6.59	6.18	6.69	6.86										
$Fe^{3+}/(Fe^{3+}+Fe^{2+})$[a]	0.373	0.373	0.373	0.373	0.373	0.373	0.373	0.373	0.373	0.373	0.373	0.373	0.373	0.373	0.373										
Fe^{3+}/Fe^{2+a}	0.595	0.595	0.595	0.595	0.595	0.595	0.595	0.595	0.595	0.595	0.595	0.595	0.595	0.595	0.595										
Fe-ratio[a]	0.37	0.38	0.37	0.38	0.41	0.41	0.4	0.4	0.39	0.4	0.42	0.41	0.38	0.4	0.43	0.37	0.37	0.37	0.38	0.35	0.36	0.35	0.32	0.38	0.35
Mg-ratio[a]	0.63	0.62	0.63	0.62	0.59	0.59	0.6	0.6	0.61	0.6	0.58	0.59	0.62	0.6	0.57	0.63	0.63	0.63	0.62	0.65	0.64	0.65	0.68	0.62	0.65

[a] Fe-ratio=Fe/(Fe+Mg); Mg-ratio=Mg/(Fe+Mg); $Fe^{3+}/(Fe^{3+}+Fe^{2+})$ was determined by Mossbauer studies; $Fe^{3+}/Fe^{2+}=0.373/(1-0.373)$; $FeO(wt.\%)=wt.\%FeO^T/(1.08\times(Fe^{3+}/Fe^{2+})+1)$; $Fe_2O_3(wt.\%)=wt.\%FeO^T-wt.\%FeO$

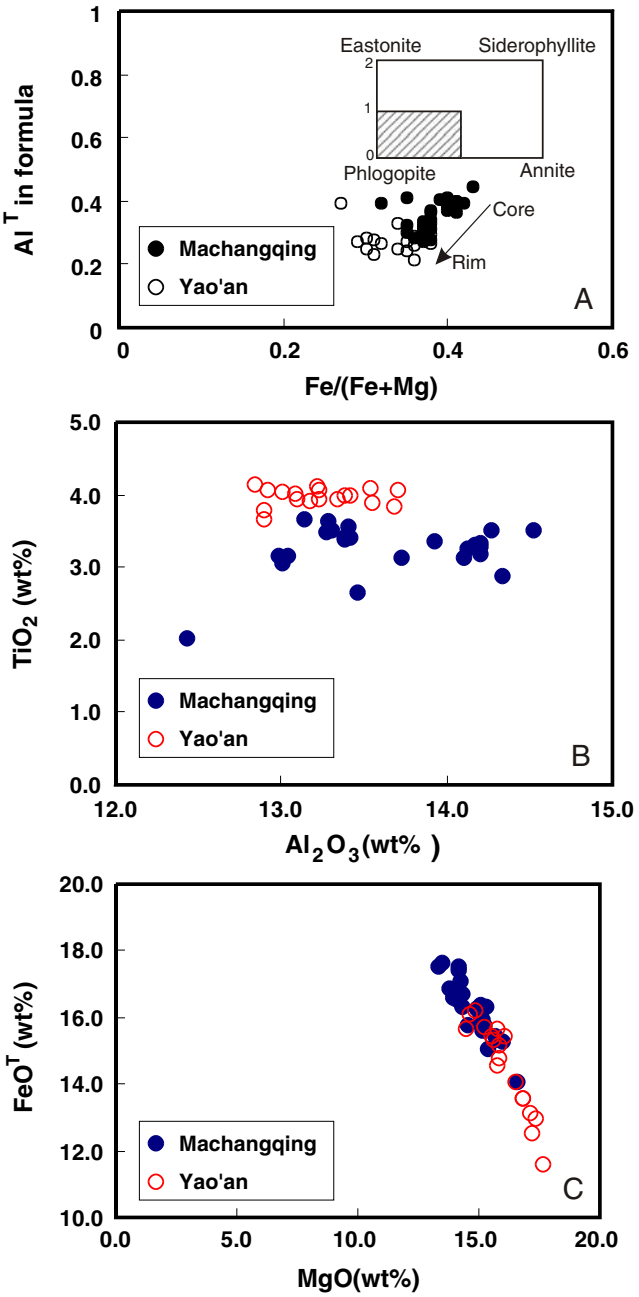

Fig. 3 Composition of biotite from the Yao'an and Machangqing alkaline intrusions. **a** Al^T vs. Fe/(Fe+Mg); **b** Al_2O_3(wt.%) vs. TiO_2(wt.%); **c** MgO(wt.%) vs. FeO^T(wt.%)

because of uncertainties related to site vacancies and charge balances (Dyar et al. 1991; Feldstein et al. 1996; Delaney et al. 1998). Thus, the total iron (FeO^T) of biotite was obtained by electron microprobe analysis, and the Fe^{3+}/Fe^{2+} ratio of biotite was determined by Mossbauer spectroscopy (Annersten 1974). Bulk mineral separates from the Yao'an and Machanqing intrusives were ground into powder in an agate mortar. Room-temperature Mossbauer studies to determine Fe^{2+} and Fe^{3+} spectra area were done in the Mossbauer Spectroscopy Laboratory at the Department of Physics in Nanjing University. The Mossbauer spectra were measured using a 25 mCi ^{57}Co/Rh source. Run times for the individual measurements averaged 1.5 days per sample. Results were calibrated against an α-Fe foil of 25 μm thickness and 99% purity.

Results

Biotite

Representative electron-microprobe analyses of biotite from the Yao'an syenite porphyry and Machangqing granite porphyry samples are listed in Tables 2 and 3 and are plotted on Fig. 3. The biotite is magnesium-rich Mg/(Fe+Mg) ranging from 0.62 to 0.73 (average 0.66) in the Yao'an syenite and from 0.57 to 0.68 (average 0.62) in the Machangqing alkali–granite. In terms of phlogopite–annite–eastonite–siderophyllite variation (Fig. 3a), biotite from both intrusions displays a low and uniform Fe/(Fe+Mg) ratio (0.34±0.07 for Yao'an and 0.38±0.06 for Machangqing) and is dominated by the phlogopite end-member. The rather uniform Fe/(Fe+Mg) ratios in the biotite rule out the possibility of modification by an overprinting late-stage fluid (Mahmood 1983; Rowins et al. 1991). As shown in Table 4 and Fig. 4, the $Fe^{3+}/(Fe^{2+}+Fe^{3+})$ ratio of the Yao'an syenite is 0.425 and 0.373 in the Machangqing alkali granite. Biotite from both intrusions (Tables 2, 3) is greatly enriched in F relative to Cl, with average F/(F+Cl) ratios of 0.91 and 0.96 for Yao'an and F/(F+Cl) ratios of 0.85 and 0.95 for Machangging.

Amphibole

Representative electron-microprobe analyses of amphibole from the Yao'an syenite and Machangqing alkali granite samples (Table 5), and plotted in Fig. 5. The amphibole is tremolite according to the classification of Hawthorne and Oberti (2006). Calcic amphibole compositions in both intrusions show increasing Al content with increasing Fe/(Fe+Mg), but are richer in Na and Ti in the Yao'an syenites than in the Machangqing alkali–granites. The Fe/(Fe+Mg) ratios of primary amphiboles are low (0.38 and 0.42) in the Machangqing alkali–granites, and range from 0.40 to 0.43 in the Yao'an syenites. Two grains of secondary actinolite of the Machangqing alkali–granite are rich in Mg, and their Fe/(Fe+Mg) ratios range from 0.24 to 0.27. Estimated $Fe^{3+}/(Fe^{3+}+Fe^{2+})$ ratios determined by the method of Cosca et al. (1991) are 0.30–0.39 in tremolite from the Machangqing alkali granite, and 0.32–0.47 in tremolite from the Yao'an syenite.

Table 4 Mössbauer parameters of biotite from Yao'an and Machangqing alkaline intrusions

Sample	χ^2	Area (%)	IS (mm/s)	QS (mm/s)	Valence	Line width (mm/s)	$Fe^{3+}/(Fe^{2+}+Fe^{3+})$
YST-35	1.1 (8)	57.5	1.1 (1)	2.3 (3)	Fe^{2+}	0.44 (5)	0.425
		29.3	0.4 (2)	0.9 (3)	Fe^{3+}	0.53 (6)	
		13.2	0.0 (4)	0.3 (9)	Fe^{3+}	0.32 (7)	
MCQ-39	1.1 (3)	62.7	1.1 (2)	2.3 (7)	Fe^{2+}	0.46 (4)	0.373
		16.5	0.3 (3)	1.0 (1)	Fe^{3+}	0.36 (5)	
		20.8	−0.0 (1)	0.3 (2)	Fe^{3+}	0.34 (0)	

YST-35 from Yao'an alkali igneous rocks, *MCQ-39* from Machangqing alkali igneous rocks

Feldspar

Representative electron-microprobe analyses of plagioclase and perthite from Yao'an syenite and Machangqing alkali granite samples are summarised in Table 6. All crystals nominally identified as plagioclase are ternary feldspars, corresponding to anorthoclase both in composition and in their typical habit and characteristic development of albite and pericline twinning. Greater extents of solid solution of Or and An components are shown by the ternary feldspars from the Yao'an syenite porphyry than the Machanquing granite porphyry.

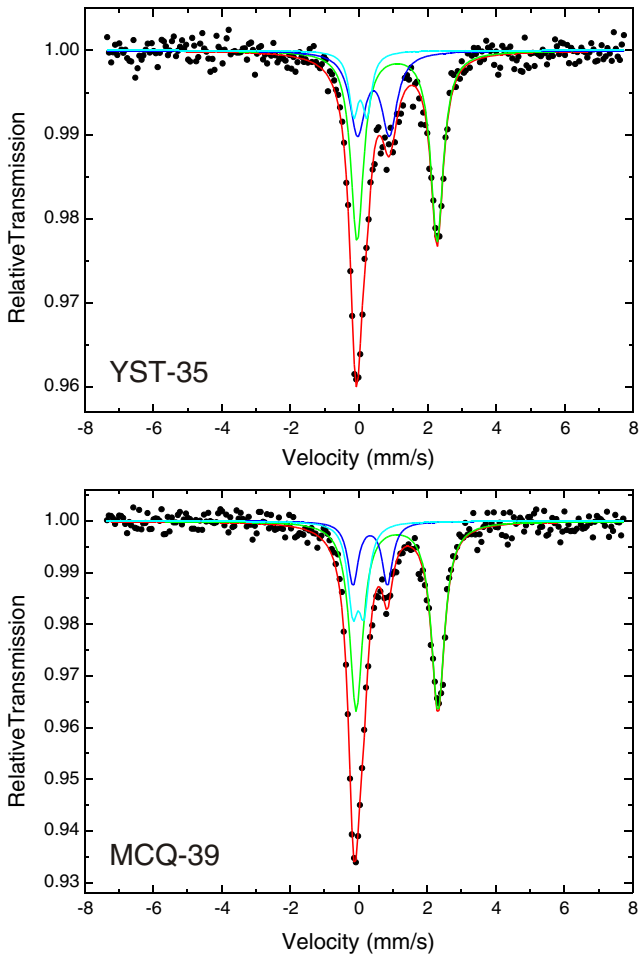

Fig. 4 Mossbauer spectra of biotite from Yao'an and Machangqing alkaline intrusions

Estimates of pressure, temperature and oxygen fugacity

Temperature–pressure

The amphibole–plagioclase thermometer of Holland and Blundy (1994) for quartz-bearing assemblages was used with the temperature-dependent formulation of the Al-in-amphibole barometer (Anderson and Smith 1995) to evaluate *T*–*P* conditions of the Machangqing alkaline intrusion. A two-feldspar thermometer (Fuhrman and Lindsley 1988) was coupled with the temperature-dependent formulation of the Al-in-amphibole barometer (Anderson and Smith 1995) to evaluate *T*–*P* conditions of emplacement of the Yao'an syenite. Anderson and Smith (1995) and Schmidt (1992) established limits in terms of Mg and Fe content of amphiboles that are suitable for Al-in-amphibole barometry. These parameters are adopted for the present study. The amphiboles are rejected for Al-in-hornblende barometry unless they have $0.4<Fe_{tot}/(Fe_{tot}+Mg)<0.65$ and $0.2<Fe^{3+}/(Fe^{3+}+Fe^{2+})$, where Mg and Fe are calculated on the basis of 13 cations. For amphibole–plagioclase thermometry, Blundy and Holland (1990) argued that this geothermometer yields temperatures of equilibration for amphibole–plagioclase assemblages with uncertainties of ±50°C for rocks equilibrated at temperatures in the range of 750–1,000°C, and will yield acceptable results only for assemblages with plagioclase less calcic than An_{92} and with amphiboles containing less than 7.8 Si atoms per formula unit.

The analysis points of co-existing phases and crystal pairs are shown in Fig. 6. Analytical data used are given in Tables 5 and 6. The temperatures for the Yao'an syenite porphyry derived from perthite–plagioclase pairs suggest crystallisation between 812°C and 824°C (Table 7). For the Machangqing pluton, amphibole–plagioclase pairs from the granite porphyry record conditions from 725°C to 733°C

Table 5 Representative electron microprobe analyses of tremolite from the Yao'an and Machangqing alkaline intrusions

	M39-5-1 inter	M39-5-1 rim	M39-5-3 rim	M39-5-4 rim	M39-5-5 rim	Y36-10-1 core	Y36-10-2 core	Y36-3-1 core	Y36-3-1 rim	Y36-3-2 core	Y36-3-2 rim	Y35-6-1 rim1	Y35-6-1 rim2	Y35-5-1 rim	Y33-11-1 rim
SiO_2	45.31	53.43	45.96	46.19	51.71	44.73	45.61	44.85	44.70	46.82	45.37	43.65	44.62	43.88	44.26
TiO_2	1.19	0.23	0.99	1.09	0.46	1.59	1.40	1.59	1.38	1.07	1.09	1.39	1.44	1.19	1.61
Al_2O_3	7.64	2.30	7.06	7.26	3.47	8.54	7.52	8.43	8.10	7.17	7.81	8.21	8.40	7.10	8.24
FeO^T	16.02	10.56	14.96	14.57	11.22	16.49	15.75	16.33	16.29	15.13	16.57	15.46	16.16	14.53	15.74
Cr_2O_3	0.00	0.02	0.00	0.00	0.06	0.04	0.09	0.07	0.03	0.01	0.02	0.00	0.05	0.00	0.05
MnO	0.51	0.17	0.60	0.47	0.18	0.38	0.36	0.34	0.38	0.39	0.38	0.34	0.35	0.35	0.45
MgO	12.48	17.24	12.85	13.14	16.47	12.43	12.85	12.66	12.53	13.15	12.43	11.69	12.30	12.47	12.43
CaO	11.32	11.67	11.32	11.29	11.77	11.16	11.17	11.26	10.89	11.08	10.94	10.48	11.15	10.52	11.01
Na_2O	1.68	0.59	1.65	1.59	0.92	2.07	2.05	2.20	2.07	2.00	2.02	1.93	2.25	1.90	2.05
K_2O	0.93	0.62	0.84	0.83	0.30	1.25	1.24	1.26	1.16	1.01	1.15	1.13	1.24	1.01	1.19
F	0.45	0.21	0.30	0.31	0.43	0.77	0.63	0.79	1.21	1.00	0.78	0.84	0.96	0.94	1.11
Cl	0.09	0.02	0.09	0.09	0.06	0.21	0.24	0.17	0.21	0.11	0.21	0.27	0.21	0.20	0.21
Total	97.63	97.03	96.61	96.83	96.97	99.60	98.82	99.88	98.91	98.94	98.75	95.39	99.10	94.09	98.29
Fe_2O_{3Calc}[a]	5.10	0.04	6.17	6.00	2.39	8.20	6.84	8.46	7.72	5.15	6.74	5.66	7.50	5.86	7.86
FeO_{Calc}[a]	10.92	10.51	8.79	8.57	8.83	8.28	8.92	7.87	8.57	9.98	9.82	9.80	8.66	8.67	7.88
$Fe^{3+}/(Fe^{2+}+Fe^{3+})$	0.30	0.004	0.39	0.39	0.20	0.47	0.40	0.49	0.45	0.32	0.38	0.34	0.44	0.39	0.47
Fe/(Fe+Mg)	0.41	0.24	0.39	0.38	0.27	0.42	0.40	0.41	0.41	0.38	0.42	0.41	0.41	0.38	0.41

[a] FeO_{Calc}, Fe_2O_{3Calc} estimations according to Cosca et al. (1991); sample number prefix "M" means Machangqing, "Y" means Yao'an

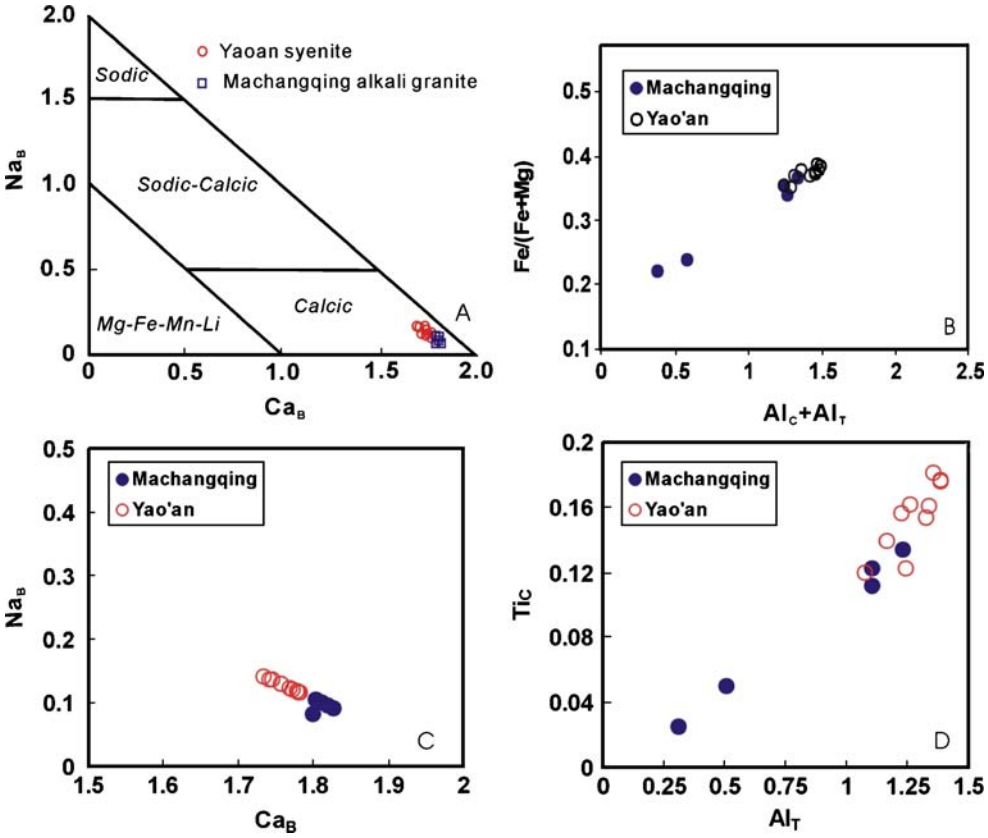

Fig. 5 Composition of amphiboles from the Yao'an and Machangqing alkaline intrusions. **a** Ca_B vs. Na_B; **b** Al_C+Al_T vs. Fe/(Fe+Mg); **c** Ca_B vs. Na_B; **d** Al_T vs. Ti_C. Abbreviations as used by Hawthorne and Oberti (2006)

Table 6 Representative electron microprobe analyses of feldspar pairs from the Yao'an and Machangqing alkaline intrusions

	SiO_2	TiO_2	Al_2O_3	FeO	MnO	MgO	CaO	Na_2O	K_2O	Total	Ab	An	Or
M39–5Ab1	65.71	0.05	20.85	0.21	0.00	0.01	1.71	9.78	1.02	99.33	85.80	8.30	5.90
M39–5Ab2	64.75	0.00	20.07	0.59	0.06	1.02	2.22	9.88	0.36	98.95	87.10	10.80	2.10
M39–5Ab3	66.35	0.00	20.76	0.17	0.02	0.00	1.61	10.83	0.31	100.05	90.80	7.40	1.70
Y36–2Ab2	62.00	0.06	22.32	0.48	0.02	0.13	3.90	7.90	1.35	98.16	72.20	19.70	8.10
Y36–2Ab1	62.88	0.00	22.98	0.15	0.00	0.00	4.08	8.23	1.40	99.71	72.20	19.80	8.10
Y35–2Ab1	63.47	0.00	22.79	0.34	0.00	0.01	3.87	8.35	1.11	99.94	74.40	19.10	6.50
Y33–3Ab1	63.50	0.03	22.05	0.17	0.04	0.01	3.34	8.64	1.75	99.51	74.20	15.90	9.90
Y33–3Ab2	63.81	0.03	22.06	0.22	0.00	0.02	3.39	8.31	1.79	99.62	73.10	16.50	10.40
Y33–1Ab2	63.86	0.02	22.70	0.25	0.04	0.00	3.71	8.50	1.52	100.60	73.60	17.80	8.70
Y33–1Ab3	61.09	0.02	22.55	0.30	0.00	0.00	4.11	7.89	1.36	97.32	71.40	20.50	8.10
Y36–2Or1	64.09	0.04	19.16	0.10	0.03	0.00	0.33	4.37	9.97	98.10	39.40	1.60	59.00
Y36–2Or2	64.42	0.06	19.30	0.14	0.00	0.00	0.34	4.38	9.72	98.36	40.00	1.70	58.30
Y35–2Or1	64.34	0.04	19.47	0.21	0.00	0.01	0.61	5.14	8.40	98.22	46.70	3.10	50.20
Y33–3Or1	63.58	0.04	19.11	0.10	0.00	0.00	0.40	4.59	9.50	97.30	41.50	2.00	56.50
Y33–3Or2	63.94	0.06	19.25	0.15	0.00	0.00	0.40	4.79	9.51	98.10	42.50	2.00	55.50
Y33–1Or2	65.78	0.06	19.42	0.07	0.00	0.00	0.21	3.34	10.08	98.96	33.10	1.20	65.70
Y33–1Or3	64.29	0.08	19.09	0.10	0.00	0.01	0.38	4.20	9.48	97.63	39.40	2.00	58.60

Note: M— Machangqing samples, Y- Yao'an samples.

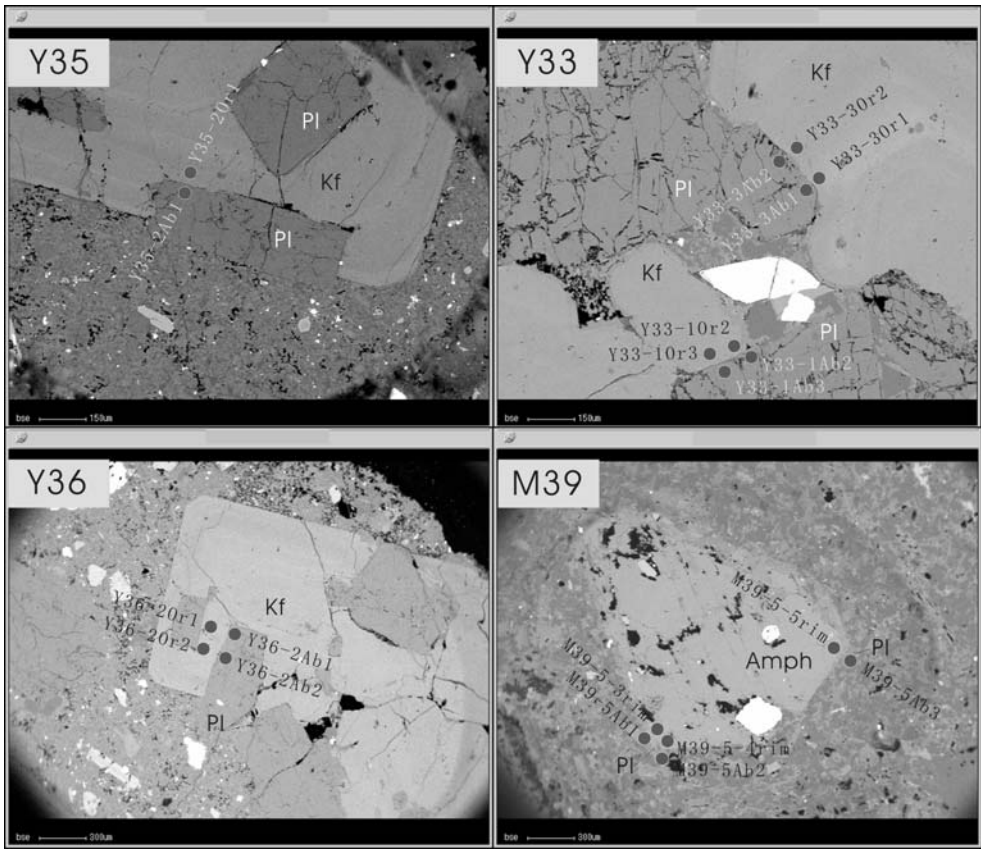

Fig. 6 Photomicrographs of the analysis points of co-existing phases of Yao'an and Machangqing alkaline intrusions. Analyses are given in Tables 5 and 6. Samples Y33-3, Y35-2, Y36-2 from Yao'an, M39-5 from Machangqing. *Amph* tremolite, *Kf* perthite, *Pl* plagioclase

(Table 7). Pressures were calculated using the following equation presented by Anderson and Smith (1995):

$$P_{\mathrm{AS}}(\pm 0.6\,\mathrm{kbar}) = 4.76\mathrm{Al}^{\mathrm{tot}} - 3.01 - ((T_{\mathrm{A}} - 675)/85) \times (0.530\mathrm{Al}^{\mathrm{tot}} + 0.005294(T_{\mathrm{A}} - 675))$$

where P_{AS} is pressure and T_{A} is temperature calculated from mineral-pair thermometers (°C). The Al content of tremolite records crystallisation pressures of 2.2–2.8 kbar within the Machangqing pluton, and 0.9–1.3 kbar within the Yao'an pluton (Table 7).

Table 7 Temperature and pressure estimates for the Yao'an and Machangqing alkaline intrusions

	Yao'an	Machangqing
n	7	3
Al_{total}	1.29–1.48	1.24–1.34
P (kbar)	0.86–1.27	2.23–2.77
T (°C)	812–824	725–733

P: Anderson and Smith (1995); T: Blundy and Holland (1990) for Machangqing, Nekvasil and Burnham (1987) for Yao'an. "n" means number of pairs.

Oxygen fugacity

The atomic proportions of Fe^{2+}, Fe^{3+} and Mg^{2+} in biotite can be used to estimate magmatic oxidation potential, where biotite occurs in textural equilibrium with magnetite and K-feldspar (Wones and Eugster 1965). Two independent sample tests of non-parametric statistical analyses were performed using SPSS 11.0 software for Fe^{2+}, Fe^{3+} and Mg^{2+} in biotite from the Yao'an syenite and Machangqing alkali–granite, and were effective in distinguishing biotite from the two intrusions ($p<0.001$ for Fe^{2+} and Fe^{3+}, $p<0.005$ for Mg^{2+}). Atomic proportions of Fe^{2+}, Fe^{3+} and Mg^{2+} for biotite from the two intrusions (Fig. 7) plot as two groups close to the hematite–magnetite (HM) buffer. According to the Fe/(Fe+Mg) ratio of biotites of two intrusions, using log $fO_2 - T$ diagram (Wones and Eugster 1965), the oxygen fugacity (fO_2) of Yao'an intrusion is about $10^{-13.0}$ bar, and those of the Machangqing intrusion is around $10^{-13.8}$ bar.

Discussion

Variations of *T*, *P*, fO_2 in the two intrusions

The temperature and pressure estimates using independent mineral equilibria for the Yao'an and Machangqing

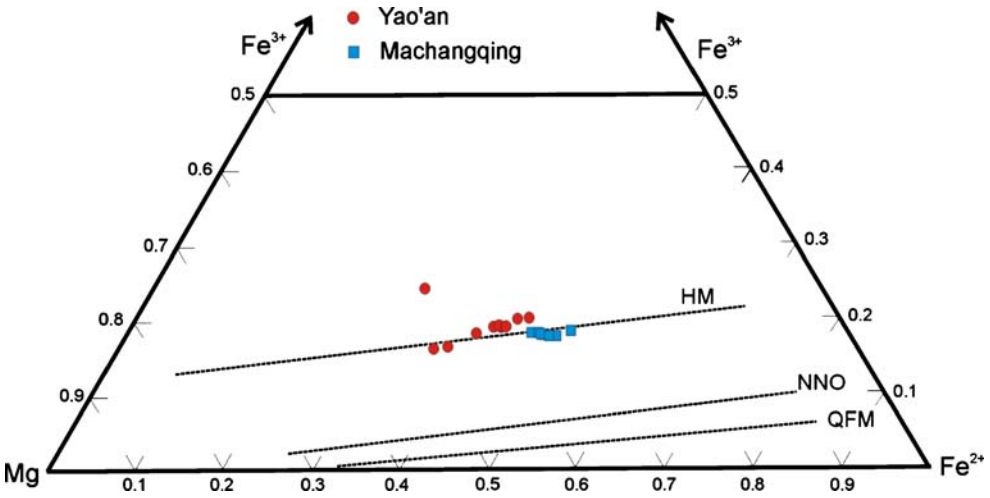

Fig. 7 Fe^{3+}–Fe^{2+}–Mg ternary diagram for the estimation of redox conditions of biotite crystallisation in the Yao'an and Machangqing alkaline intrusions. *Dashed lines* represent fO_2 buffers. Experimentally derived fO_2 buffer after Wones and Eugster (1965). *Dark square* and *dark dot* represent the samples (see Tables 2 and 3)

intrusions show that the syenite porphyry in the Yao'an intrusion crystallised at 820±50°C (perthite–plagioclase pairs), and 0.9–1.3 kbar, and the alkali–granite porphyry in the Machangqing intrusion crystallised at conditions around 730±50°C (hornblende–plagioclase pairs), and 2.2–2.8 kbar. Biotite from both porphyries, especially from Yao'an, is greatly enriched in F relative to Cl. The high F/(F+Cl) ratios are broadly consistent with biotite which has not experienced secondary recrystallisation in the presence of late stage or evolved, lower temperature hydrothermal fluids which typically results in enrichment in Cl relative to F (Zhu and Sverjensky 1991). The higher temperature and lower pressure for the Yao'an intrusion indicates that it was emplaced at relatively shallower levels in the crust compared to the Machangqing intrusion.

The biotite chemistry suggests that both intrusions crystallised at oxygen fugacities well above the NNO buffer (Fig. 7), which is more than two log units above FMQ (Mungull 2002). Thus like in arc magmas with a high potential to generate Au and Cu deposits (Ballard et al. 2002; Mungall 2002; Richards 2003), the alkaline magmas associated with Cu–Au mineralisation in the continental setting in Southwestern China also record relatively high fO_2. The oxygen fugacity estimates presented here suggest that the Yao'an syenite formed at a relatively higher oxygen fugacity compared with the Machangqing alkali–granite throughout their crystallisation intervals.

Redox controls on Au and Cu behavior in magma

The oxygen fugacity of a magma controls the oxidation state of sulfur in a melt. At low oxygen fugacity, sulfur in the magma exists mainly as S^{2-}, which has a relatively low solubility in silicate melts (Katsura and Nagashima 1974; Carroll and Rutherford 1985, 1988). Sulfur saturation is more easily reached in reduced magmas and the precipitation of sulfides in these magmas would be expected to occur earlier than in oxidised ones (Carroll and Rutherford 1985, 1988). Chalcophile elements, such as Cu and Au, would be partitioned into these early sulfides and not concentrated into late stage melts and the magmatic–hydrothermal fluid (Blevin 2004). At high oxygen fugacity, sulfur in the magma is mainly present as oxidised sulfur species (e.g. SO_2), which have a much higher solubility in silicate melts than reduced sulfur species (e.g. H_2S, Carroll and Rutherford 1985, 1988), and will tend to delay or even prevent saturation of a magmatic sulfide phase. Thus, copper and gold will accumulate in the melt during differentiation under oxidised conditions, and be concentrated into a magmatic–hydrothermal fluid (Ballard et al. 2002).

In the Red River–Jinshajiang alkaline intrusive suite, a clear genetic link has been established between alkaline potassic intrusions and spatially associated gold and copper mineralisation by Hu et al. (1998, 2004) and Bi et al. (2000, 2002, 2004). The He, Ar, S, C isotope and REE data suggest that the mineralising fluids were derived from the volatile-rich alkaline intrusions. The Yao'an and Machangqing alkaline intrusions associated with porphyry Cu–Au deposits were emplaced at high fO_2, on the basis of biotite composition (Fig. 7). It is concluded therefore that oxidation state is also a key factor in determining the potential of alkaline magmas for forming Cu–Au mineralization in the Red River–Jinshajiang alkaline intrusive belt.

Fractionation of felsic magma may concentrate gold so long as it behaves as an incompatible element. Gold may be removed from magmas by the crystallisation of sulfides, particularly intermediate solid solution (iss), and to a lesser extent, magnetite (Cygan and Candela 1995; Simon et al. 2003). Compatible behaviour and the removal of gold may be limited by low sulfur content, low iron content, or high oxidation state leading to sulfate stability (Thompson et al.

1999). Crystallisation at high fO_2 promotes the incompatible behaviour of gold and assists in its efficient partitioning into a magmatic fluid phase. Transport of gold within an orthomagmatic fluid from a cooling intrusion into a fracture stockwork can lead to the deposition of gold in restricted volumes of rock to form an ore deposit. At lower fO_2, sulfide minerals or even sulfide melt may separate from the silicate magma, effectively stripping the magma of its gold before it can generate an orthomagmatic aqueous fluid (Mungall 2002; Richards 2003).

As discussed above, the gold-related Yao'an syenite crystallised under more oxidizing conditions, with a weaker degree of fractionation, compared to the Machangqing alkaline granite that hosts copper mineralization. The combination of limited extent of fractional crystallisation and a high fO_2, probably sufficiently oxidising to stabilize oxidized sulfur species in the melt, allowed the magma at Yao'an to evolve to the point of saturation with an aqueous fluid without suffering significant loss of gold. On the other hand, lower fO_2 and a greater extent of fractional crystallisation have apparently resulted in significant reductions in the gold content of the Machangqing magma before the separation of an orthomagmatic fluid, leading to copper-dominated mineralisation instead. This is in agreement with the results of a study of Au-rich and Au-poor copper porphyry-type deposits by Sillitoe (1998).

Conclusions

The two alkaline intrusions associated with porphyry Cu–Au deposits described here, were emplaced at high fO_2. This implies that oxidation state is a key factor in determining the potential of alkaline magmas for forming Cu–Au mineralisation in continental tectonic settings.

Two distinct evolutionary paths are recognized for the magmas parental to the Au–Cu-mineralised Yao'an syenite and the Cu-mineralised Machangqing alkali granite, despite their similar origins in metasomatised upper mantle lithosphere. The Yao'an syenite records a limited history of fractional crystallisation at shallow depths, comparatively high temperatures, and higher fO_2, before it solidified and exsolved a Au- and Cu-rich, highly-oxidising orthomagmatic fluid. The Machangqing alkali–granite records a more extensive process of fractional crystallisation to relatively lower temperature at greater depth, and lower fO_2, and exsolved a Au-poor and Cu-rich orthomagmatic fluid.

Acknowledgements This work was supported jointly by the Chinese Academy of Sciences Innovational Program (KZCX2-YW-111-02, KZCX2-YW-Q04-01), National Basic Research Program of China (2009CB421005), the National Natural Sciences Foundations of China (40673042, 40373020) and the Natural Sciences and Engineering Research Council of Canada. We gratefully acknowledge Dr C. Cermignani of the Department of Geology, University of Toronto, Canada for his assistance with the electron microprobe. Reviews by Peter Downes and the Editors Lalou G. Gwalani and Johann G. Raith greatly improved the manuscript.

References

Ague JJ (1997) Thermodynamic calculation of emplacement pressures for batholithic rocks, California: implications for the aluminum-in-hornblende barometer. Geology 25:563–566

Anderson JL, Smith DR (1995) The effects of temperature and fO_2 on the Al-in-hornblende barometer. Am Mineral 80:549–559

Annersten H (1974) Mossbauer studies of natural biotites. Am Mineral 59:143–151

Ballard JR, Palin JM, Campbell IH (2002) Relative oxidation states of magmas inferred from Ce(IV)/Ce(III) in zircon: application to porphyry copper deposits of northern Chile. Contrib Mineral Petrol 144:347–364

Bi XW (1999) Study on alkali-rich intrusive rocks and their relation with metallogenesis of copper and gold in the "Sanjiang" region, western Yunnan. Ph.D. thesis, Institute of Geochemistry, Chinese Academy of Sciences, Guiyang (in Chinese)

Bi XW, Hu RZ, Ye ZJ, Shao SX (2000) Relations between A-type granites and copper mineralization as exemplified by the Machangqing Cu deposit. Sci China Ser D 43:93–102

Bi XW, Cornell DH, Hu RZ (2002) The origin of altered fluid: REE evidence from primary and secondary feldspars in the mineralization–alteration zone. Ore Geol Rev 19:69–78

Bi XW, Hu RZ, Cornell DH (2004) Trace element and isotope evidence for the evolution of ore-forming fluid of Yao'an gold deposit, Yunnan province, China. Miner Depos 39:21–30

Bi XW, Hu RZ, Peng JT, Wu KX, Su WC, Zhan XZ (2005) Geochemical characteristics of the Yao'an and Machangqing alkaline intrusions. Petrol Acta(1):113–124

Blevin PL (2004) Redox and compositional parameters for interpreting the granitoid metallogeny of eastern Australia: implications for gold-rich ore systems. Res Geol 54:241–252

Blundy JD, Holland TJB (1990) Calcic amphibole equilibria and a new plagioclase amphibole geothermometer. Contrib Mineral Petrol 104:208–224

Bonin B (2007) A-type granite and related rocks: evolution of a concept, problems and prospects. Lithos 97:1–29

Carroll MR, Rutherford MJ (1985) Sulfide and sulfate saturation in hydrous silicate melts. J Geophys Res 90:C601–C612

Carroll MR, Rutherford MJ (1988) Sulfur speciation in hydrous experimental glasses of varying oxidation state: results from measured wavelength shifts of X-rays. Am Mineral 73:845–849

Chung SL, Lee TY, Lo CH, Wang PL, Cheng CY, Yem NT, Hoa TT, Wu GY (1997) Intraplate extension prior to continental extrusion along the Ailao Shan–Red River shear zone. Geology 25:311–314

Chung SL, Lo CH, Lee TY, Zhang YQ, Xie YW, Li XH, Wang LW, Wang PL (1998) Diachronous uplift of the Tibetan plateau starting 40Myr ago. Nature 394:769–773

Cosca MA, Essene EJ, Bowman JR (1991) Complete chemical analyses of metamorphic hornblendes: implications for normalizations, calculated H_2O activities, and thermobarometry. Contrib Mineral Petrol 108:472–484

Cygan GL, Candela PA (1995) Preliminary study of gold partitioning among pyrrhotite, pyrite, magnetite, and chalcopyrite in gold-saturated chloride solutions at 600 to 700°C, 140 MPa (1400 bars). In: Thompson JFH (ed) Magmas, fluids, and ore deposits. Min Assoc Can Short Course Ser 23:129–137

Delaney JS, Dyar MD, Sutton SR, Bajt S (1998) Redox ratios with relevant resolution: solving an old problem by using the synchrotron micro XANES probe. Geology 26:139–142

Deng WM, Huang X, Zhong DL (1998) Petrological characteristics and genesis of Cenozoic alkali-rich porphyry in west Yunnan, China. Science Geologica Sinica 33:412–425 (in Chinese with English abstract)

Dyar MD, Colucci MT, Guidotti CV (1991) Forgotten major elements—hydrogen and oxygen variation in biotite from metapelites. Geology 19:1029–1032

Elliott BA, Rämö OT, Nironen M (1998) Mineral chemistry constraints on the evolution of the 1.88–1.87 Ga post-kinematic granite plutons in the Central Finland Granitoid Complex. Lithos 45:109–129

Elliott BA (2001) Crystallization conditions of the Wiborg rapakivi batholith, SE Finland: an evaluation of amphibole and biotite mineral chemistry. Mineral Petrol 72:305–324

Feldstein SN, Lange RA, Vennemann T, O'Neil JR (1996) Ferric–ferrous ratios, H_2O contents and D/H ratios of phlogopite and biotite from lavas of different tectonic regimes. Contrib Mineral Petrol 126:51–66

Fuhrman ML, Lindsley DH (1988) Ternary-feldspar modeling and thermometry. Am Mineral 73:201–215

Garrio I, Cembrano J, Siña A, Stedman P, Yánez G (2002) High magma oxidation state and contractional deformation: key factors in the generation of Andean porphyry copper deposits, Central Chile (31–43°S). Rev Geol Chile 29:3–14

Ghent ED, Nicholls J, Simony PS, Sevigny JH, Stout MZ (1991) Hornblende barometry of the Nelson batholith, southeastern British Columbia: tectonic implications. Can J Earth Sci 28:1982–1991

Hawthorne, FC, Oberti, R (2006) On the classification of amphiboles. Can Mineral 44:1–21

Holland T, Blundy J (1994) Non-ideal interactions in calcic amphiboles and their bearing on amphibole–plagioclase thermometry. Contrib Mineral Petrol 116:433–447

Holliday JR, Wilson AJ, Blevin PL, Tedder IJ, Dunham PD, Pfitzner M (2002) Porphyry gold–copper mineralization in the Cadia district, eastern Lachlan Fold Belt, New South Wales, and its relationship to shoshonitic magmatism. Miner Depos 37:100–116

Hou ZQ, Ma HW, Khin Z, Zhang YQ, Wang MJ, Wang Z, Pan GT, Tang RL (2003) The Himalaya Yulong poyphyry copper belt: product of large-scale strike–slip faulting in eastern Tibet. Econ Geol 98:125–145

Hou ZQ, Pan XF, Yang ZM, Qu XM (2007) Porphyry Cu–(Mo–Au) deposits no related to oceanic-slab subduction: examples from Chinese porphyry deposits in continental settings. Geoscience 21:332–351

Hu XZ, Huang Z (1997) The petrology and petrogensis of the Yangtze platform western margin's alkali-rich granite porphyry. Geotectonica et Metallogenia 21:173–180 (in Chinese with English abstract)

Hu RZ, Burnard PG, Turner G, Bi XW (1998) Helium and argon isotope systematics in fluid inclusions of Machangqing copper deposit in west Yunnan province, China. Chem Geol 146:55–63

Hu RZ, Burnard PG, Bi XW, Zhou MF, Peng JT, Su WC, Wu KX (2004) Helium and argon isotope geochemistry of alkaline intrusion-associated gold and copper deposits along the Red River–Jingshajiang fault belt, SW China. Chem Geol 203:305–317

Imai A, Listanco EL, Fuji T (1993) Petrologic and sulfur isotopic significance of highly oxidized and sulfur-rich magma of Mount Pinatubo, Philippines. Geology 21:699–702

Ishihara S (1981) The granitoid series and mineralization. Econ Geol 75th Anniversary Volujme:458–484

Katsura T, Nagashima S (1974) Solubility of sulfur in magma. Geochim Cosmochim Acta 38:517–531

Leloup PH, Laccassin R, Tapponnier P, Schärer U, Zhong DL, Liu X, Zhang LS, Ji S, Phan TT (1995) The Ailaoshan–Red River shear zone (Yunnan, China), Tertiary transform boundary of Indochina. Tectonophysics 251:3–84

Liang HY, Campbell IH, Allen C, Sun WD, Liu CQ, Yu HX, Xie YW, Zhang YQ (2006) Zircon Ce^{4+}/Ce^{3+} ratios and ages for Yulong ore-bearing porphyries in eastern Tibet. Miner Depos 41:152–159

Loferski PJ, Ayuso A (1995) Petrography and mineral chemistry of the composite Deboullie pluton, northern Maine, U.S.A.: implications for the genesis of Cu–Mo mineralization. Chem Geol 123:89–105

Lowenstern JB (1991) Evidence for extreme partitioning of copper into a magmatic vapor phase. Science 252:1405–1409

Ludington S (1978) The biotite–apatite geothermometer revisited. Am Mineral 63:551–553

Mahmood A (1983) Chemistry of biotites from a zoned granitic pluton in Morocco. Mineral Mag 47:364–369

Maughan DT, Keith JD, Christiansen EH, Pulsipher T, Hattori K, Evans NJ (2002) Contributions from mafic alkaline magmas to the Bingham porphyry Cu–Au–Mo deposit, Utah, USA. Miner Depos 37:14–37

Mungall JE (2002) Roasting the mantle: slab melting and the genesis of major Au and Au-rich Cu deposits. Geology 30:915–918

Nekvasil H and Burnham CW (1987) The calculated individual effects of pressure and water content on phase equilibria in the granite system. In: Mysen BO (ed) Magmatic processes: physicochemical principles. Geochem Soc Spec Publ 1:433–445

No. 301 Team of Southwest Geological Exploration Bureau (1981) The geological exploration report of Machangqing copper deposit, Yunnan province

No. 304 Team of Southwest Geological Exploration Bureau (1995) The geological exploration report of Yao'an gold deposit, Yunnan province

Peng JT, Bi XW, Hu RZ, Wu KX, Sang HQ (2005) Determination of ore- and rock-forming time of the Machangqing porphyry Cu (Mo) deposit, western Yunnan province. Acta Mineralogica Sinica 25:69–74

Pollard PJ, Taylor RG (2002) Paragenesis of the Grasberg Cu–Au deposit, Irian Jaya, Indonesia: results from logging section 13. Miner Depos 37:117–136

Richards JP (1995) Alkalic-type epithermal gold deposits: a review. Mineral Assoc Can Short Course Ser, Mineral Soc Can, pp 376–406

Richards JP (2003) Tectono-magmatic precursors for porphyry Cu–(Mo–Au) deposit formation. Econ Geol 98:1515–1533

Rowins SM, Lalonde AE, Cameron EM (1991) Magmatic oxidation in the syenitic Murdock Creek intrusion, Kirkland lake, Ontario: evidence from the ferromagnesian silicates. J Geol 99:395–414

Rui ZY, Zhang LS, Chen ZY, Wang LS, Liu YL, Wang YT (2004) Approach on source rock or source region of porphyry copper deposits. Acta Petrolei Sinica 20:229–238

Schmidt MW (1992) Amphibole composition in tonalite as a function of pressure: an experimental calibration of the Al-in-hornblende barometer. Contrib Mineral Petrol 110:304–310

Selby D, Nesbitt BE (2000) Chemical composition of biotite from the Casino porphyry Cu–Au–Mo mineralization, Yukon, Canada: evaluation of magmatic and hydrothermal fluid chemistry. Chem Geol 171:77–93

Sillitoe RH (1997) Characteristics and controls of the largest porphyry copper–gold and epithermal gold deposits in the circum-Pacific region. Aust J Earth Sci 44:373–388

Sillitoe RH (1998) Major regional factors favoring large size, high hypogene grade, elevated Au content and supergene oxidation and enrichment of porphyry copper deposit. In: Porter TM (Ed) Porphyry and hydrothermal Cu and Au deposits—a global perspective. Conf Proc Aust Mineral Found, pp 21–34

Sillitoe RH (2002) Some metallogenic features of gold and copper deposits related to alkaline rocks and consequences for exploration. Miner Depos 37:4–13

Simon AC, Pettke T, Candela PA, Piccoli PM, Heinrich CA (2003) Experimental determination of Au solubility in rhyolite melt and magnetite: constraints on magmatic Au budgets. Am Mineral 88:1644–1651

Stewart RB, Price RC, Smith IEM (1996) Evolution of high-K arc magma, Egmont volcano, Taranaki, New Zealand: evidence from mineral chemistry. J Volcanol Geotherm Res 74:275–295

Stone D (2000) Temperature and pressure variations in suites of Archean felsic plutonic rocks, Berens river aera, northwest Superior province, Ontario, Canada. Can Mineral 38:455–470

Sun WD, Arculus RJ, Kamenetsky VS, Binns RA (2004) Release of gold-bearing fluids in convergent margin magmas prompted by magnetite crystallization. Nature 431:975–978

Thompson JFH, Sillitoe RH, Baker T, Lang JR, Mortensen JK (1999) Intrusion-related gold deposits associated with tungsten–tin provinces. Miner Depos 34:323–334

Tu GC, Zhang YQ, Zhao ZH (1984) A preliminary study on the two alkali-rich intrusive rock belts in South China. In: Xu KQ (ed) Geology of granites and its relations with mineralization. Jiangsu Science and Technology Press, Jiangsu, pp 21–37 (in Chinese)

Turner S, Arnaud N, Liu J, Rogers N, Hawkesworth C, Harris N, Kelley S, VanCalsteren P, Deng W (1996) Post-collision, shoshonitic volcanism on the Tibetan plateau: implications for convective tinning of the lithosphere and the source of ocean island basalts. J Petrol 37:45–71

Vyhnal CR, McSween HY, Speer JA (1991) Hornblende chemistry in southern Appalachian granitoids: implications for aluminum hornblende thermobarometry and magmatic epidote stability. Am Mineral 76:176–188

Wang PL, Lo CH, Lee TY, Chung SL, Lan CY, Yem NT (1998) Thermochronological evidence for the movement of the Ailaoshan–Red river shear zone: a perspective from Vietnam. Geology 26:887–890

Wang JH, Harrison TM, Grove M, Zhang YQ, Xie GH (2001) A tectonic model for Cenozoic igneous activities in the eastern Indo-Asian collision zone. Earth Planet Sci Lett 188:123–133

Wang DH, Qu WJ, Li ZW, Yin HL, Chen YC (2005) Mineralization episode of porphyry copper deposits in the Jinshajiang–Red River mineralization belt: Re–Os dating. Sci China Ser D Earth Sci 48:192–198 (in Chinese)

Wones DR, Eugster HP (1965) Stability of biotite: experiment, theory, and application. Am Mineral 50:1228–1272

Xie YW, Zhang YQ (1995) Compositional characteristics and petrological significance of Mg–Fe micas in alkalic rocks of the Red River–Jinshajiang rift system. Acta Mineralogica Sinica 15:81–87 (in Chinese with English abstract)

Yin A, Harrison TM (2000) Geologic evolution of the Himalayan–Tibetan orogen. Annu Rev Earth Planet Sci 28:211–280

Zhang LS, Schärer U (1999) Age and origin of magmatism along the Cenozoic Red River shear belt, China. Contrib Mineral Petrol 134:67–85

Zhang YQ, Xie YW, Tu GC (1987) A preliminary study on the relationship between rift and Ailaoshan–Jianshajiang alkaline intrusive rocks. Acta Petrolei Sinica 3:17–25 (in Chinese with English abstract)

Zhang YQ, Xie YW, Tu GC (1997) Nd, Sr isotopic character and chronology of Red River–Jinshajiang alkali-rich intrusive rocks. Sci China 27:289–293 (in Chinese)

Zhu C, Sverjensky DA (1991) Partitioning of F–Cl–OH between minerals and hydrothermal fluids. Geochim Cosmochim Acta 55:1837–1858